La mer 33, 63–75, 1995
Société franco-japonaise d'océanographie, Tokyo

A numerical experiment on the path dynamics of the Kuroshio south of Japan Part 1. Coastal topographic effect*

Mingqiu ZHANG** and Yoshihiko SEKINE**

Abstract: Effects of the coastal topography on the path dynamics of the Kuroshio are studied by use of a two layer numerical model. Realistic coastal topographies south of Japan with a flat bottom is employed as Part 1 of this study. A straight path is formed when in- and outflow volume transport is relatively small (30 Sv). If the in- and outflow volume transport of 55 Sv is given, two cyclonic eddies southeast of Kyushu and Kii Peninsula and two anti-cyclonic eddies southwest of Kyushu and south of Shikoku are formed and a large meander path is formed. It is shown from vorticity balance that advection term is balanced with the planetary beta term in offshore region, while the advection term is balanced with the friction term near the coastal boundary. If in- and outflow volume transport of 70 Sv is given, more amplified large meander path is formed. However, if the in- and outflow volume transport is increased to 80 Sv, a different flow pattern with the dominant eastward flow from south of Kyushu is formed. It is pointed out that a critical maximum volume transport exists for the generation of large meander path. In the cases with large meander path, current path commonly separates from the Cape Muroto. If only the coastal topography corresponding to the Kii Peninsula is excluded from the numerical model, separation point of the mean flow at the Cape Muroto is not changed. However, the separation point shifts to east of the Cape Muroto, if the coastal topography corresponding to the Cape Muroto is excluded. If both coastal topographies of the Cape Muroto and Kii Peninsula are excluded, the separation point shifts further downstream. It is resulted that the topographic effect of the Cape Muroto has an important influence on the path dynamics of the Kuroshio south of Japan.

1. Introduction

The kuroshio south of Japan is a western boundary current of the subtropical circulation in the North Pacific. It has been widely accepted that the Kuroshio has a bimodal path characteristics between a straight path and a large meander path (e.g., TAFT, 1972; NITANI, 1975; ISHII *et al.*, 1983). There have been various studies on the bimodal path dynamics of the Kuroshio. In early studies (e.g. WHITE and MCCREARY, 1976; CHAO and MCCREARY, 1982; MASUDA, 1982), the Kuroshio takes large meander path when the volume transport and/or the current velocity of the Kuroshio is relatively small, because the large meander of the Kuroshio is considered essentially as a stationary Rassby wave in the zonal flow. In contrast to these studies, it is shown by some later studies (e.g. YOON and YASUDA, 1987; SEKINE, 1988; 1990; AKITOMO *et al.*, 1991) that the Kuroshio takes the large meander path when the volume transport is relatively large. The difference between the early and later studies is the inclusion of topographic effect of northern coastal topography inclination from zonal direction in the later studies. In particular, AKITOMO *et al.* (1991) showed important topographic effects of Kyushu and Kii Peninsula on the path dynamics of the Kuroshio. They also showed that these topographies give mean flow the positive vorticity, which is necessary for the generation of large meander path. However, because coastal topographies south of

* Received December 7, 1994
** Institute of Oceanography, Faculty of Bioresources, Mie University, 1515, Kamihama, Tsu, Mie, 514 Japan

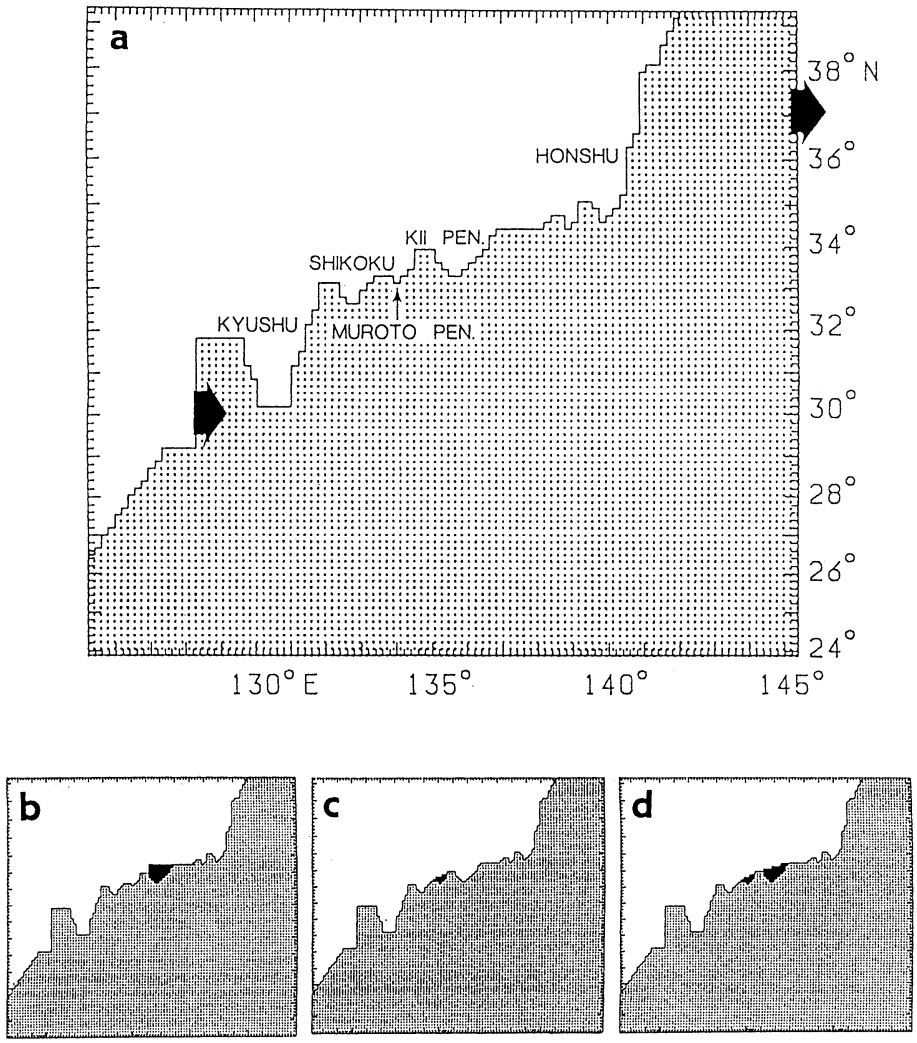

Fig. 1. (a) Domain of numerical experiments (stippled area) of F30, F55, F70 and F80 shown in Table 2. (b) Domain of FKN55, (c) FMN55 and (d) FMKN55. Closed areas in (b), (c) and (d) are excluded from the domain of (a). Two arrows in (a) indicate the boundary with in- and outflow.

Japan are significantly simplified in their model, details of the coastal topographic effects south of Japan were not fully discussed.

In the present study, we model more realistic topographies south of Japan and examine the coastal and bottom topographic effects on the path dynamics of the Kuroshio. As Part 1 of this study, we assume a flat bottom ocean with a depth of 3800 m and coastal topographic effects on the path dynamics of the Kuroshio are examined. The bottom topographic effects of the continental slope and Izu Ridge will be discussed in Part 2 of this study (ZHANG and SEKINE, 1995). In the following, model characteristics are described in the next section, results of numerical experiments in section 3 and summary and discussion in section 4.

2. Numerical model

A two layer ocean is assumed and the upper layer and lower layer have a constant density ρ and $\rho + \Delta\rho$, respectively. We adopt a

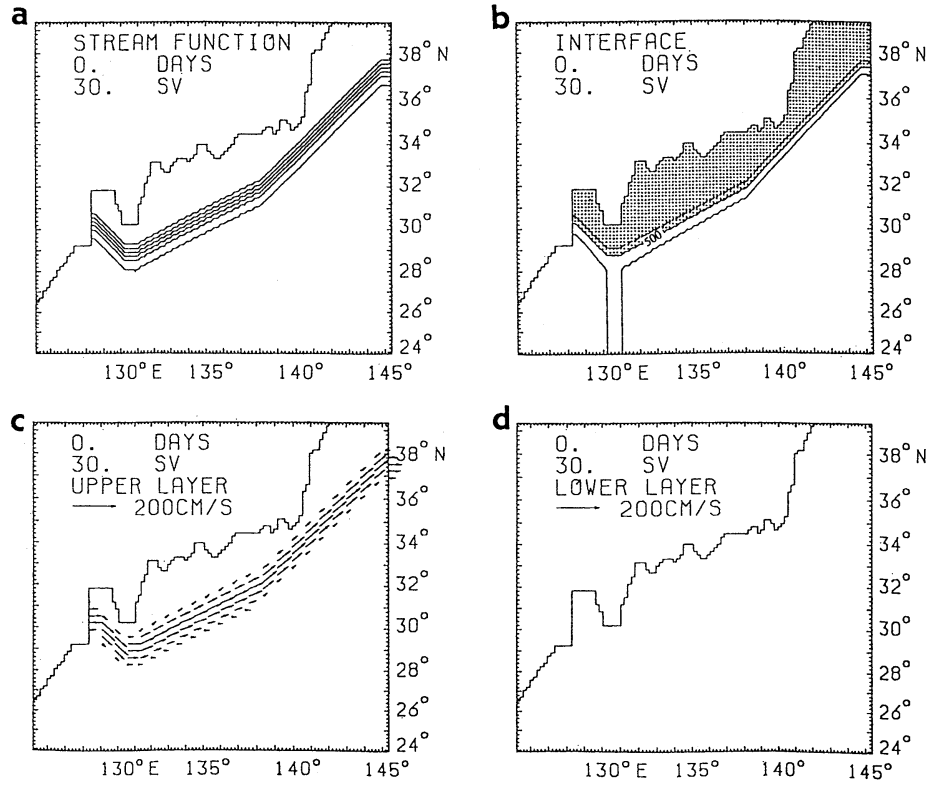

Fig. 2. Initial condition of F30. (a) Spatial distribution of volume transport function, (b) upper layer thichness, (c) velocity fields of upper layer and (d) those of lower layer. The contour intervals of the volume transport function and the upper layer thickness are 5 Sv and 50 m, respectively. Areas with negative volume transport or thinner upper layer thickness less than 500 m are stippled.

Cartesian coordinate system on a β plane with x-axis to east, y-axis to north and z-axis to upward. The vertically integrated equations for a two-layer Boussinesq fluid in hydrostatic balance are

$$\begin{cases} \dfrac{\partial u_1 h_1}{\partial t} = -\dfrac{\partial u_1^2 h_1}{\partial x} - \dfrac{\alpha u_1 v_1 h_1}{\partial y} - \dfrac{\rho}{\rho_0} g h_1 \dfrac{\partial \zeta}{\partial x} \\ \qquad + f v_1 h_1 + A_h \nabla^2 u_1 h_1 \qquad (1) \\ \dfrac{\partial u_1 h_1}{\partial t} = -\dfrac{\partial u_1 v_1 h_1}{\partial x} - \dfrac{\partial v_1^2 h_1}{\partial y} - \dfrac{\rho}{\rho_0} g h_1 \dfrac{\partial \zeta}{\partial y} \\ \qquad + f u_1 h_1 + A_h \nabla^2 v_1 h_1 \qquad (2) \\ \dfrac{\partial h_1}{\partial t} = -\dfrac{\partial u_1 h_1}{\partial x} - \dfrac{\partial v_1 h_1}{\partial y} \qquad (3) \end{cases}$$

$$\begin{cases} \dfrac{\partial u_2 h_2}{\partial t} = -\dfrac{\partial u_2^2 h_2}{\partial x} - \dfrac{\partial u_2 v_2 h_2}{\partial y} - \dfrac{\rho}{\rho_0} g h_2 \dfrac{\partial \zeta}{\partial x} \\ \qquad + \dfrac{\Delta\rho}{\rho_0} g h_2 \dfrac{\partial \eta}{\partial x} + f v_2 h_2 + A_h \nabla^2 u_2 h_2 \qquad (4) \\ \dfrac{\partial v_2 h_2}{\partial t} = -\dfrac{\partial \alpha u_2 h_2}{\partial x} - \dfrac{\partial v v_2 h_2}{\partial y} - \dfrac{\rho}{\rho_0} g h_2 \dfrac{\partial \zeta}{\partial y} \\ \qquad + \dfrac{\Delta\rho}{\rho_0} g h_2 \dfrac{\partial \eta}{\partial y} + f v_2 h_2 + A_h \nabla^2 v_2 h_2 \qquad (5) \\ \dfrac{\partial h_2}{\partial t} = -\dfrac{\partial u_2 h_2}{\partial x} - \dfrac{\partial v_2 h_2}{\partial y} \qquad (6) \end{cases}$$

where

$$h_1 = H + \eta, \quad \zeta \ll \eta, H, \qquad (7)$$

$$h_2 = D - H - \eta. \qquad (8)$$

The rigid lid approximation is assumed and we introduce the total volume transport function

$$\begin{cases} u_1h_1+u_2h_2=-\dfrac{\partial\phi}{\partial y}, & (9)\\ \nu_1h_1+\nu_2h_2=\dfrac{\partial\phi}{\partial x}. & (10)\end{cases}$$

Then, the equations (1)-(6) are transformed into the vorticity equation for the barotropic mode with a flat bottom ocean:

$$\boxed{\frac{\partial Z}{\partial t}} = \boxed{\begin{array}{l} -\dfrac{\partial}{\partial x}\left\{\dfrac{1}{D}\left(\dfrac{\partial}{\partial x}u_1\nu_1h_1+\dfrac{\partial}{\partial y}\nu_1^2h_1\right)\right\}+\dfrac{\partial}{\partial y}\left\{\dfrac{1}{D}\left(\dfrac{\partial}{\partial x}u_1^2h_1+\dfrac{\partial}{\partial y}u_1\nu_1h_1\right)\right\} \\ -\dfrac{\partial}{\partial x}\left\{\dfrac{1}{D}\left(\dfrac{\partial}{\partial x}u_2\nu_2h_2+\dfrac{\partial}{\partial y}\nu_2^2h_2\right)\right\}+\dfrac{\partial}{\partial y}\left\{\dfrac{1}{D}\left(\dfrac{\partial}{\partial x}u_2^2h_2+\dfrac{\partial}{\partial y}u_2\nu_2h_2\right)\right\} \end{array}}$$

Total change — Advection

$$\text{Beta term}\quad \boxed{-\frac{\beta\partial\phi}{D\partial x}} + \boxed{A_h\nabla^2Z} \quad \text{Friction} \qquad (11)$$

and shear equation for the baroclinic mode:

$$\frac{\partial S_u}{\partial t} = -\frac{\Delta\rho}{\rho_0}g\frac{\partial\eta}{\partial x}+fS_\nu+A_h\nabla^2A_u - \frac{\partial u_1^2}{\partial x}-\frac{\partial u_1\nu_1}{\partial y}+\frac{\partial u_2^2}{\partial x}+\frac{\partial u_2\nu_2}{\partial y}, \qquad (12)$$

$$\frac{\partial S_\nu}{\partial t} = -\frac{\Delta\rho}{\rho_0}g\frac{\partial\eta}{\partial y}-fS_u+A_h\nabla^2A_\nu - \frac{\partial u_1\nu_1}{\partial x}-\frac{\partial\nu_1^2}{\partial y}+\frac{\partial u_2\nu_2}{\partial x}+\frac{\partial\nu_2^2}{\partial y}, \qquad (13)$$

where

$$Z=\frac{\partial}{\partial x}\left(\frac{1\partial\phi}{D\partial x}\right)+\frac{\partial}{\partial y}\left(\frac{1\partial\phi}{D\partial y}\right) \qquad (14)$$

$$\begin{cases} S_u=u_1-u_2 & (15)\\ S_\nu=\nu_1-\nu_2 & (16)\end{cases}$$

The continuity equation for the above system is

$$\frac{\partial\eta}{\partial t}=\frac{\partial h_2u_2}{\partial x}+\frac{\partial h_2\nu_2}{\partial y} \qquad (17)$$

The symbols used in the above equations are tabulated in Table 1. Schematic view of the model ocean is shown in Fig.1. The system is driven by in- and outflow through the open boundary. For the initial state, the flow is given only in the upper layer and the lower layer has no motion (Fig. 2). Sinusoidal horizontal velocity distribution of in- and outflow is assumed and only eastward velocity component is given at the boundaries:

$$(u_1,\ \nu_1)=\left(u_0\sin\left\{\frac{\pi}{L}y\right\},\ 0\right), \qquad (18)$$

$$(u_2,\ \nu_2)=(0,\ 0). \qquad (19)$$

Table 1. List of symbols

t	time
u_i(i=1, 2)	velocity in the x-direction
v_i(i=1, 2)	velocity in the y-direction
h_i(i=1, 2)	layer thickness
η	interface deviation positive downward from mean interface level
D	total depth ($D=3.8\times10^5$cm)
H	mean upper layer thickness ($H=4.0\times10^4$cm)
ζ	surface deviation from average surface level
f	Coriolis parameter ($f_0=6.19\times10^{-5}$sec^{-1})
β	linear change rate of the Coriolis parameter in the y-direction ($\beta=2\times10^{13}$ cm sec^{-1})
g	acceleration due to gravity (g=980cm sec^{-2})
g^*	reduced gravity ($g^*(\Delta\rho/\rho_0)\times g=2.87$ cm sec^{-2})
ρ_0	mean density over the upper and lower layer
$\Delta\rho$	density difference between upper and lower layer
A_h	horizontal eddy viscosity coefficient ($A_h=10^7$cm^2 s^{-1})
Subscripts 1 and 2	quantities in the upper and lower layer, respectively

Table 2. Parameters, in- and outflow transport, coastal topographies for the experments discussed in this study

Runs	Volume transport of in- and outflow (Sv)	Maximum Velocity of inflow u_0(cm sec^{-1}) in (18)	Topography of Kii Peninsula	Topograhpy of Cape Muroto
F30	30	61.9	Yes	Yes
F55	55	100.7	Yes	Yes
F70	70	121.1	Yes	Yes
F80	80	133.7	Yes	Yes
FKN55	55	100.7	No	Yes
FMN55	55	100.7	Yes	No
FMKN55	55	100.7	No	No

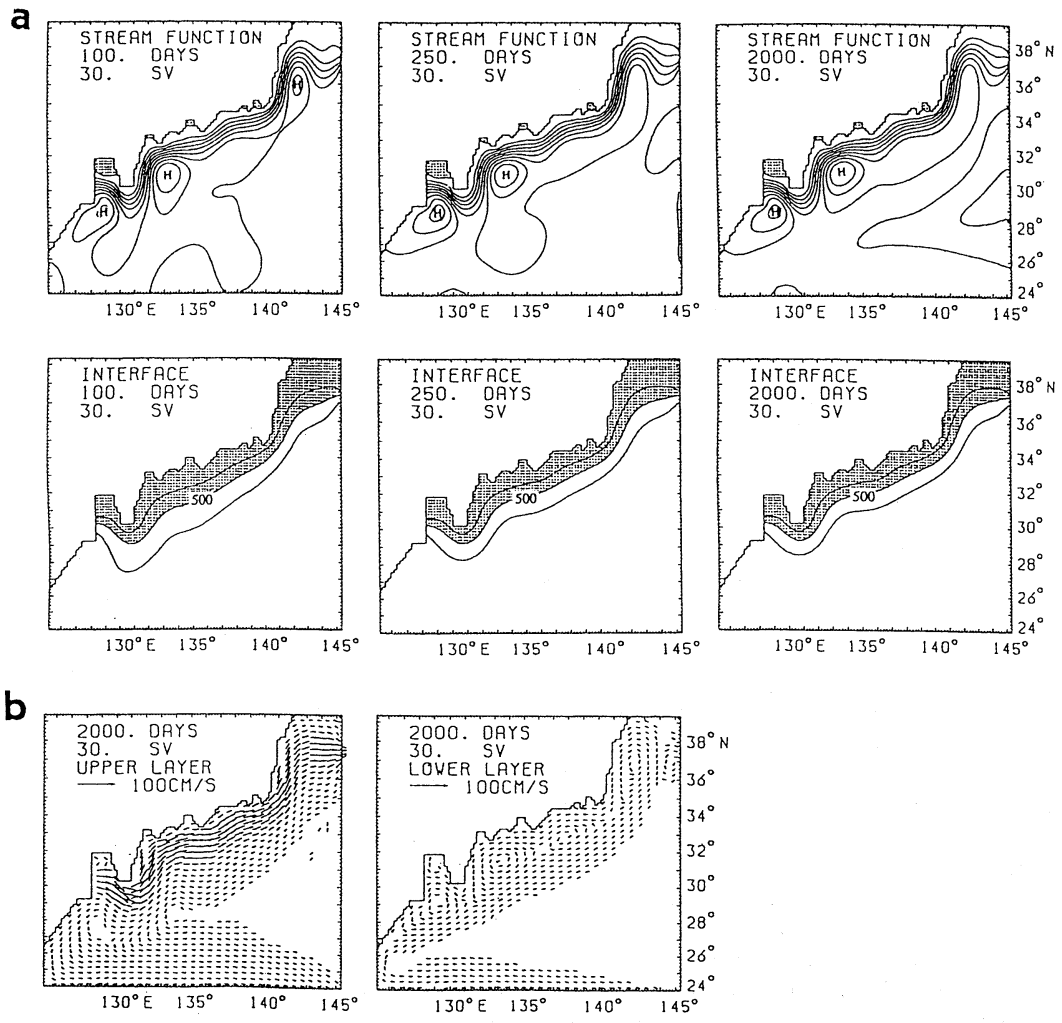

Fig. 3. Result of F30 shown by (a) volume transport function (upper) and the upper layer thickness (lower) and (b) upper and lower layer velocity fields. The contour interval in (a) is the same as in Fig. 2. No velocity vectors less than 5 cm sec^{-1} are plotted.

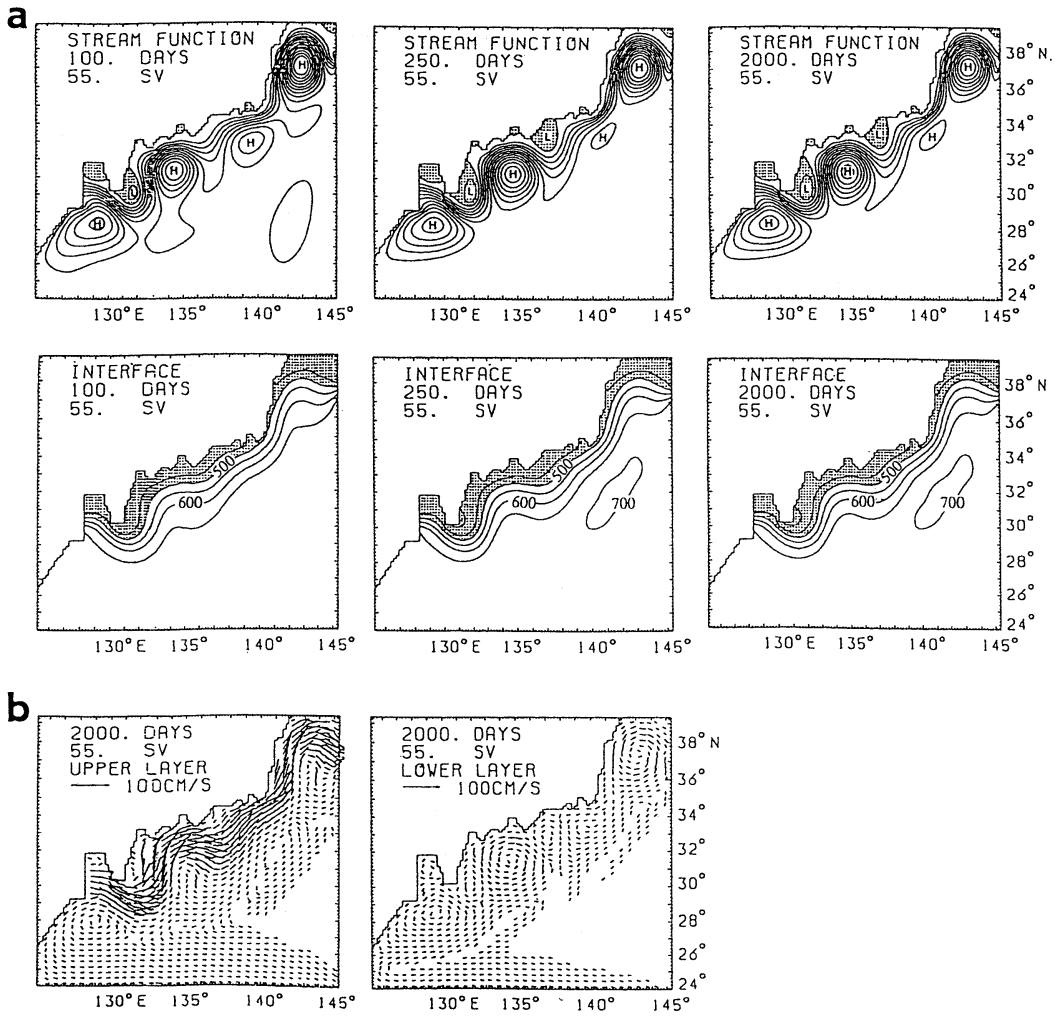

Fig. 4. Same as in Fig. 3 but for F55. The contour interval of the volume transport function is 10 Sv.

Where L=158 Km is the width of in- and outflow, u_0 is the maximum velocity at the center of in- and outflow. Viscous boundary condition is imposed on the northern boundary and slip condition is imposed on the other open boundaries. In the numerical calculation, we adopt a rectangular grid with horizontal spacing of 18.7 Km along x - axis and 15.8 Km along y - axis.

In the present study, seven cases of numerical experiments with defferent model character are performed (Table 2). Firstly, the realistic coastal topography shown in Fig. 1 is assumed and different in- and outflow volume transport of 30 Sv (1 Sv = 10^{12} cm^3sec^{-1}), 55 Sv, 70 Sv and 80 Sv are given, which are referred as F30, F55, F70 and F80, respectively. Secondly, to see the specified topographic effect of Cape Muroto and Kii Peninsula, additional three experiments are performed: the coastal topography of Kii Peninsula is excluded in FKN55 (Fig. 1b). In next, the coastal topography of Cape Muroto is excluded in FMN55 (Fig. 1c) and both Cape Muroto and Kii Peninsula are excluded in FMKN55 (Fig. 1d) . These models are driven by the in- and outflow with the volume transport of 55 Sv. The horizontal velocity distribution of in- and outflow at the boundaries is similar to all experiments and u_0 in (18) is

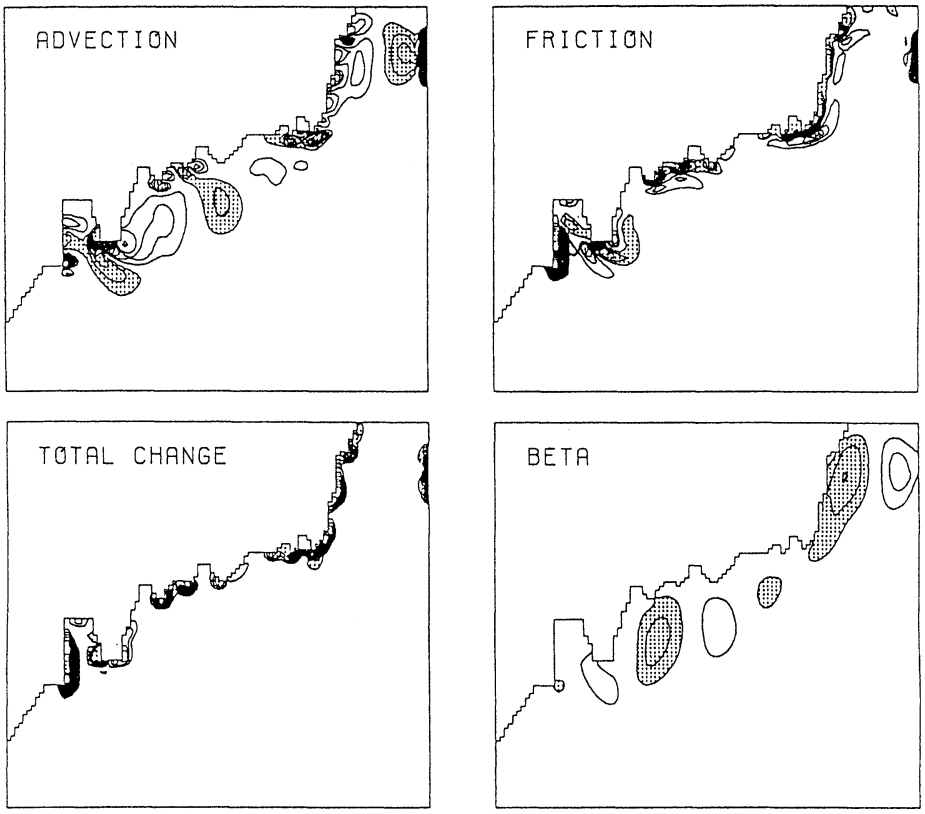

Fig. 5. Spatial distribution of vorticity change in Eq. (11) for F55 averaged over 1500–2000 days. The contour interval is 1.5×10^{-12} s^{-2} and regions with negative value less than -1.5×10^{-12} s^{-2} are stippled.

listed in Table 2.

3. Results

The result of F30 is shown in Fig. 3. The current path is stable and flows along northern boundary. The velocity fields (Fig. 3b) show that the upper layer flow runs along the northern boundary. Some anti-cyclonic circulations are detected in southwest of Kyushu, off Shikoku and off Enshu-nada in the lower layer. The result of F55 (Fig. 4) shows that two cyclonic eddies are formed in southeast of Kyushu and east of Kii Peninsula and total flow pattern shows an observed large meander path after about 250 days. This large meander path is stable and maintained stationary. It is showed from the velocity fields (Fig. 4b) in the upper layer that two separation of the current path are detected at southeast of Kyushu and at east of Kii Peninsula. In the lower layer, two cyclonic circulation southeast of Kyushu and east of Kii Peninsula are more enhanced in comparison with F30. In order to see basic dynamics of a large meander path of F55, spatial distribution of the vorticity change in Eq. (11) is shown in Fig. 5. It is shown that the friction term is mainly balanced with advection term near the coastal boundary, but the planetary beta term is mainly balanced with advection term in offshore region. It is resulted that obtained large meander path is essentially considered as a stationary Rossby wave. It should be noticed that the advection of negatibe vorticity from Cape Muroto is prominent, which shows that current path separates from Cape Muroto and forms the large meander path by the planetary beta effect.

Almost similar flow pattern to F55 is de-

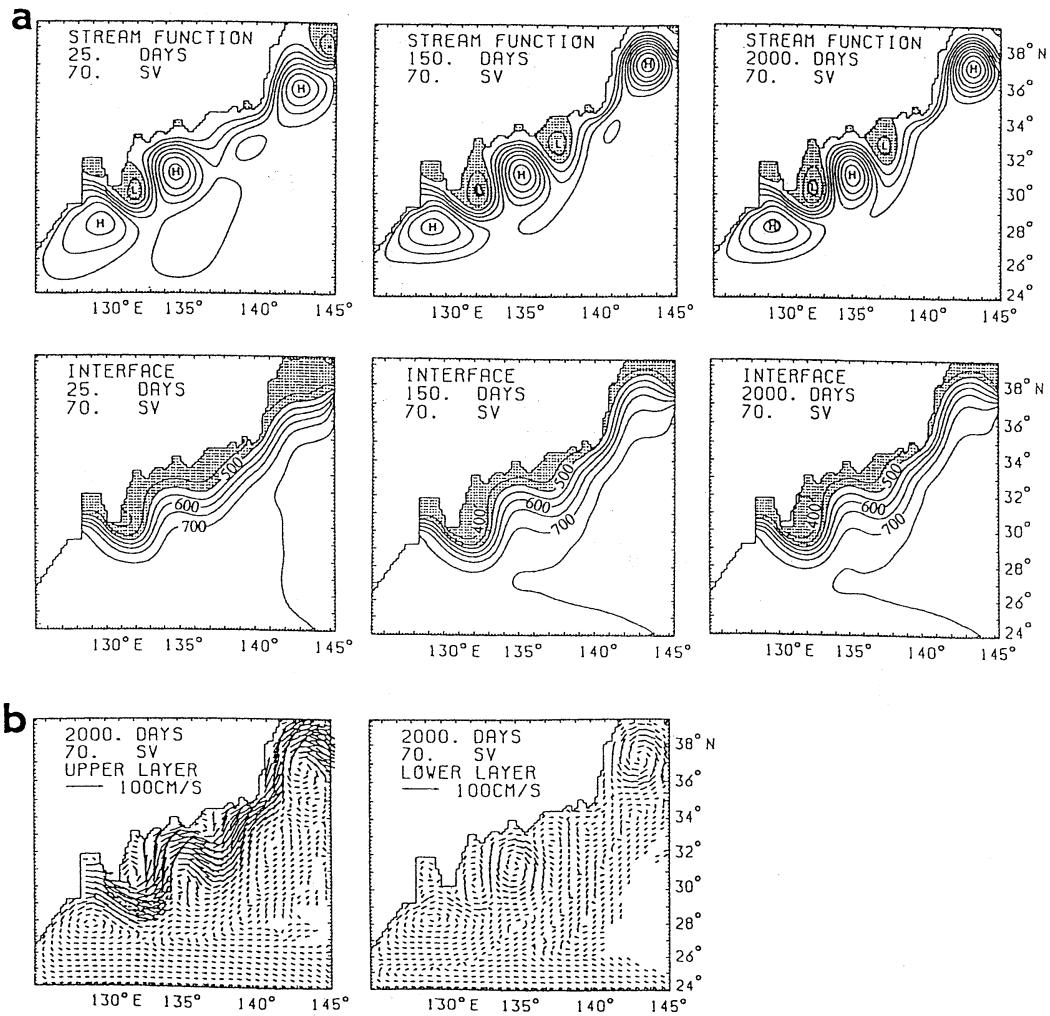

Fig. 6. Same as in Fig. 3 but for F70. Contour interval of the volume transport function is 20 Sv.

tected in F70 (Fig. 6). However, the large meander path is relatively amplified. The volume transport of two cyclonic eddies southeast of Kyushu and Kii Peninsula are about 48 Sv and 28 Sv, while those of F55 are 19 Sv and 7 Sv, respectively.

Enhanced large meander path is also generated in early stage of F80 (Fig. 7.) However, after about 250 days, the cyclonic eddy southeast of Kyushu is weakened and a northward flow east of Kyushu is changed to flow eastward. This eastward flow is further developed and it runs zonal direction to southeast of Kii Peninsula. Conversely, the cyclonic eddy off Kii Peninsula shifts westward and a weak wide cyclonic area is formed in the northern side of zonal flow. Anti-cyclonic circulation develops on southern side of the zonal flow. Because this zonal flow is due to large eastward advection by the mean flow, this flow is considered as a new flow pattern that exists in larger nonlinear (inertial) stage than the large meander stage appeared in F55 and F70. It is suggested that there exists a critical maximum in- and outflow volume transport and/or current velocity for the generation of large meander path.

Spatial distribution of volume transport

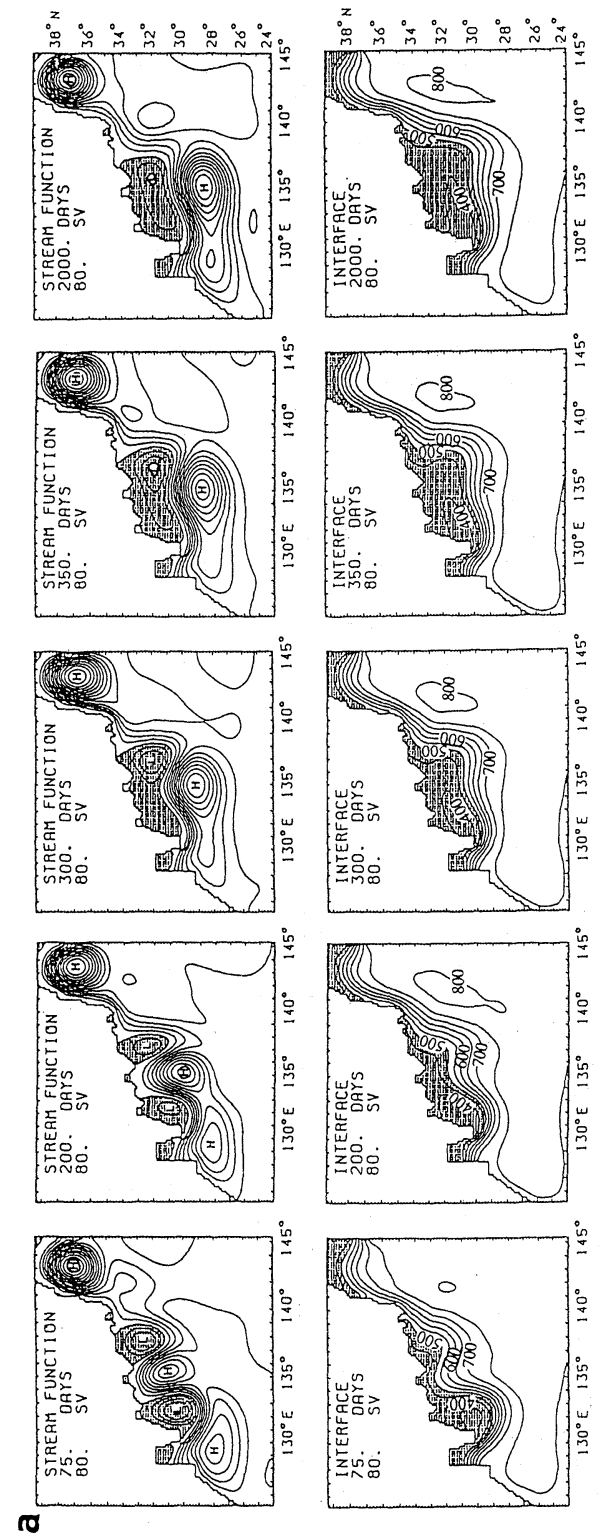

Fig. 7. Same as in Fig. 6 but for F80.

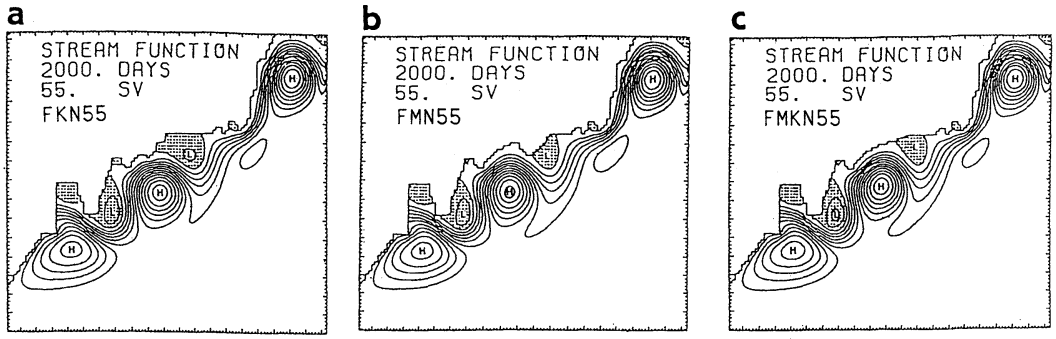

Fig. 8. Results shown by the horizontal distribution of volume transport function. (a) FKN55, (b) FMN55 and (c) FMKN55. The contour interval is 10 Sv and regions with negative value are stippled.

function of FKN55 is shown in Fig. 8a. Although large meander path is almost similar to F55, volume transport of the cyclonic eddy off Kii Peninsula with 12 Sv is larger than that of F55 (7Sv). It is shown from the spatial distribution of vorticity change (Fig. 9a) that the advection of negative vorticity from Cape Muroto is very significant, which suggests that current path separates at Cape Muroto.

To see this more clearly, the contours of 10 Sv, which represents the northern latitude of the mean flow, is shown in Fig. 10. It is noted that almost common spacial distribution of 10 Sv contour is detecetd between F55 and FKN55. It is thus resulted that the separation point at the Cape Muroto is not changed, even if the coastal topography of Kii Peninsula is excluded. Result of FMN55 (Fig. 8b) shows that the current path runs along the northern boundary off Shikoku. In comparison with the flow pattern of F55 (Fig. 4), current path off Cape Muroto shifts to further northeastward. The spatial distribution of the vorticity change (Fig. 9b) shows the advection of negative vorticity from Kii Peninsula. it is indicated from Fig. 10 that the separation of the current path of FMN55 shifts downstream in comparison with F55. The eastward shift of the separation point is more enhanced in FMKN55. It is concluded that the separation point of the current path shifts eastward, if the coastal topography of Cape Muroto is excluded, however, the separation point is not changed if the kii Peninsula is excluded.

4. Summary and discussion

We have examined the coastal topographic effect south of Japan on the path dynamics of the Kuroshio path. As a Part I of this study, a flat bottom model with a depth of 3800 m is assumed. The main results are summarized as follows:

(1) Only a stationary straight path is formed, if in- and outflow volume transport is 30 Sv. However, a large meander path is formed, if in- and outflow volume transport of 55～70 Sv is given. It is shown from spatial distribution of the vorticity change that advection term is balanced with friction term near the northern boundary, while advection term is balanced with planetary beta term in offshore region. The large meander path is considered as a stationary Rossby wave.

(2) In case with in- and outflow volume transport of 80 Sv, dominant zonal flow from south of Kyushu to southeast of Kii Peninsula is formed by the large eastward advection of the main flow. It is shown that there exists a critical maximum in- and outflow volume transport and/or current velocity for the generation of a large meander path.

(3) If the topography of Kii Peninsula is excluded from the model, large meander path is almost similar to the case with realistic coastal topography and separation point of the current path from the northern boundary is not changed. However, if the topography of Cape Muroto is excluded, separation point shifts to downstream. It is resulted that the current

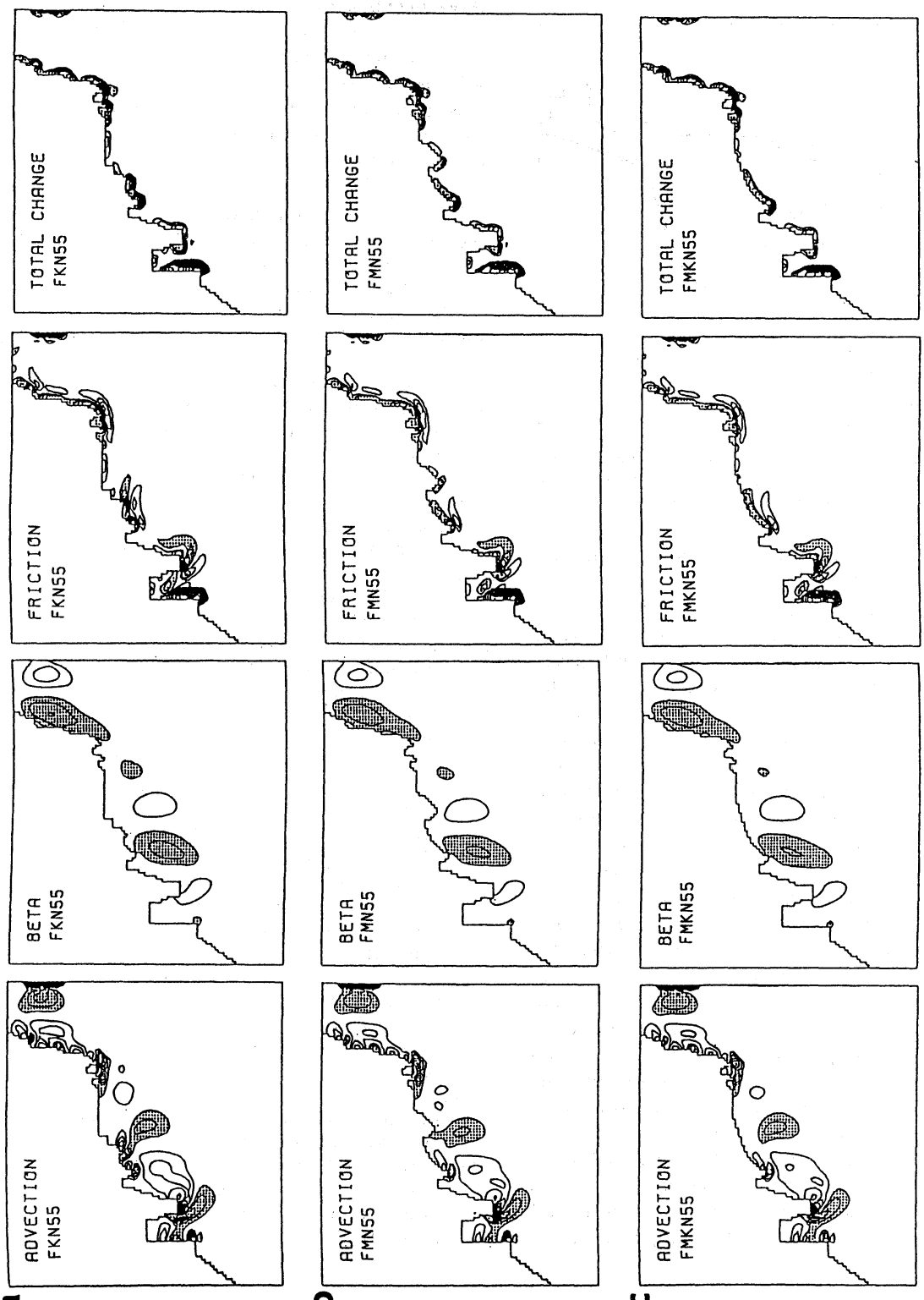

Fig .9. Same as in Fig. 5 bur for (a) FKN, (b) FMN55 and (c) FMKN55. The contour interval is 1.5×10^{-12} sec^{-2} for (a) 5×10^{-13} sec^{-2} for (b) and (c). Regions with negative value less than -1.5×10^{-12} sec^{-2} for (a) and 5×10^{-13} sec^{-2} are stippled.

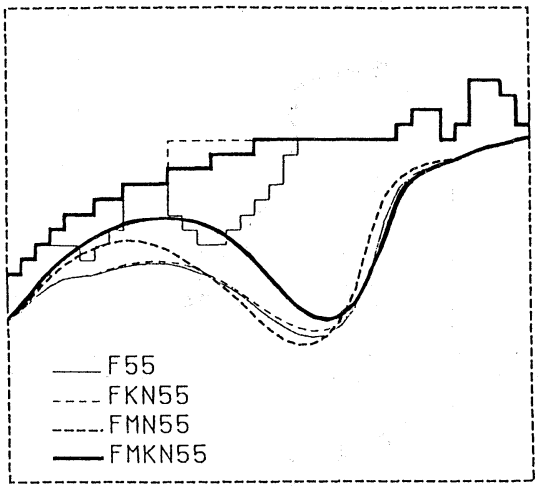

Fig. 10. Contour of the 10 Sv volume transport, which represents the northern most latitude of the mean flow. Coastal topographies for each model are also shown.

path has a strong tendency to separate at Cape Muroto.

In the above results a large meander path is formed when the volume transport is relatively large in the present study. This result agrees with the later studies (YOON and YASUDA, 1987; SEKINE, 1988, 1990; AKITOMO *et al.* 1991) with inclined coastal topography south of Japan. It is pointed out that the inclusion of northern coastal topography from east-west direction is necessary for the investigation of the path dynamics of the Kuroshio south of Japan.

YAMAGATA and UMATANI (1989) and AKITOMO *et al.* (1991) showed the important topographic effect of Kii Peninsula for a large meander path. However, it is shown from this study that large meander path usually separates from Cape Muroto. It is needed to consider the details of the coastal topographic effects south of Japan on the actual path dynamics of the Kuroshio. Although only the coastal topographic effect has been studied in the present study, topographic effect of the bottom slope is also important for the path dynamics of the Kuroshio. As the Part II of this study, the topographic effect of the continental slope south of Japan and Izu Ridge will be examined.

Acknowledgment.

The numerical calculations were carried out on a VP-2600 of Nagoya University and on a FACOM M-760 of Mie University. This study was supported by a Graind in Aid for Scientific Research from the Ministry of Education, Science of Culture of Japan (05640475).

Reference

AKITOMO, K., T. AWAJI and N. IMASATO (1991): Kuroshio path variation south of Japan. 1 Barotropic inflow-outflow model. J. Geophys. Res., **96**, 2549–2560.

CHAO, S. Y and J. P. MCCREARY (1982): A numerical study of the Kuroshio south of Japan. J. Phys. Oceanogr., **12**, 680–693.

ISHII, H., Y. SEKINE and Y. TODA (1983): Hydrographic structure of the Kuroshio large-cold water mass region down to the deeper layers of the ocean. J. Oceanogr. Soc. Japan, **39**, 240–250.

MASUDA, A (1982): An interpretation of the bimodal character of the stable Kuroshio path. Deep-sea Res., **29**, 471–484.

NITANI, H. (1975): Variation of the Kuroshio south of Japan. J. Oceanogr. Soc. Japan, **31**, 154–173.

SEKINE, Y. (1988): Coastal and bottom topographic effects on the path dynamics of the west boundary current with special reference to the Kuroshio south of Japan. La mer, **26**, 99–114.

SEKINE, Y. (1990): A numerical experiment on the path dynamics of the Kuroshio with reference to the formation of the large meander path south of Japan. Deep-sea Res., **37**, 359–380.

TAFT, B.A. (1972): Characteristics of the flow of the Kuroshio south of Japan. In: Kuroshio - Its physical aspects, H. Stommel and K. Yoshida, editors, Univ. Tokyo Press, pp. 165–214.

WHITE, W.B. AND J.P. MCCREARY (1976): The Kuroshio meander and its relation-ship to the large scale ocean circulation. Deep-Sea Res., **23**, 33–47.

YAMAGATA, T. and S. UMATANI (1989): Geometry-forced coherent structure as a model of the Kuroshio large meander. J. Phys. Oceanogr., **19**, 130–138.

YOON J. H. and I. YASUDA (1987): Dynamics of the Kuroshio large meander. Two-layer model. J. Phys. Oceanogr., **17**, 66–81.

ZHANG, M. and Y. SEKINE (1995): A numerical experiment on the path dynamics of the Kuroshio south of Japan. Part 2 Bottom topographic effect. La mer **33**, 77–87.

日本南岸の黒潮流路の力学に関する数値実験

第1部　陸岸地形効果

張　銘秋・関根義彦

要旨：二層数値モデルを用いて日本南岸の黒潮流路の力学に関する陸岸地形効果を調べた．この研究の第1部として，3800mの平坦な海底を仮定した．流出入の流量が30Svの場合には直進流路が生じる．流出入流量が55Svの場合には九州の南東と紀伊半島の南東に低気圧渦が形成され，大蛇行流路が生じる．渦度バランスの解析により，冲では移流項と惑星ベータ項と，岸近くでは移流項と粘性項がバランスしていることが示された．流出入流量が70Svの場合にはより振幅の大きい大蛇行流路が生じた．しかし，流出入流量が80Svの場合には九州の南から東進する流路が生じ，大蛇行流路の形成については流量（流速）の上限があることが示された．大蛇行流路が生じたモデルでは室戸岬から流路が離岸した．紀伊半島に陸岸地形を取り去ったモデルでは室戸岬の流路の離岸は変わらないが，室戸岬を取り去ったモデルでは離岸する点が室戸岬より東に移動した．紀伊半島と室戸岬の陸岸地形を取り去ったモデルでは離岸する点はさらに東の下流に移動する．黒潮には室戸岬の陸岸地形が重要な役割を果たしていることが示された．